Tunable Protease-Activatable Virus Nanonodes

Justin Judd,[†] Michelle L. Ho,[†] Abhinav Tiwari,[†] Eric J. Gomez,[†] Christopher Dempsey,[†] Kim Van Vliet,[§] Oleg A. Igoshin,[†] Jonathan J. Silberg,[‡] Mavis Agbandje-McKenna,[§] and Junghae Suh[†,*]

[†]Department of Bioengineering and [‡]Department of Biochemistry and Cell Biology, Rice University, Houston, Texas 77005, United States, and [§]Department of Biochemistry and Molecular Biology, University of Florida, Gainesville, Florida 32611, United States

ABSTRACT We explored the unique signal integration properties of the self-assembling 60-mer protein capsid of adeno-associated virus (AAV), a clinically proven human gene therapy vector, by engineering proteolytic regulation of virus—receptor interactions such that processing of the capsid by proteases is required for infection. We find the transfer function of our engineered protease-activatable viruses (PAVs), relating the degree of proteolysis (input) to PAV activity (output), is highly nonlinear, likely due to increased polyvalency. By exploiting this dynamic polyvalency, in combination with the self-assembly properties of the virus capsid, we show that mosaic PAVs can be constructed that operate under a digital AND gate regime, where two different protease inputs are required for virus activation. These results show viruses can be engineered as signal-integrating nanoscale nodes whose functional properties are regulated by multiple proteolytic signals with easily tunable and predictable response surfaces, a promising development toward advanced control of gene delivery.

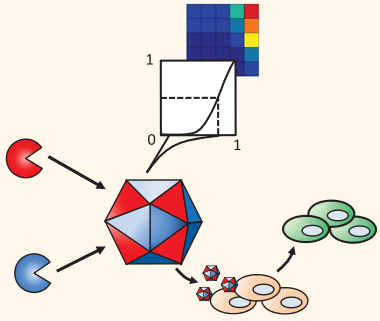

KEYWORDS: gene delivery · matrix metalloproteinase · logic gate · adeno-associated virus · mosaic capsid

Modular molecular information processing can often be achieved through protein assemblies, which serve to integrate otherwise freely diffusible signals and is amenable to facile evolution and synthetic reengineering.[1] Although largely unexplored as hubs for signal integration, virus nanoparticle platforms offer several attractive features (*e.g.*, monodispersity, multivalency, genetic design, geometry, and self-assembly) which have led to their use in diverse applications such as battery design,[2] photon harvesting,[3] piezoelectric energy conversion,[4] medical imaging,[5] reaction compartmentalization,[6,7] and intercellular communication.[8] In this study, we sought to investigate the ability of adeno-associated virus (AAV) capsids to integrate biomolecular information in the form of proteases.

Proteases play complex roles throughout mammalian physiology in diverse processes including matrix turnover and remodeling and extra- and intracellular signaling involved in cell cycle progression, apoptosis, and immune cell extravasation and migration (reviewed in ref 9). Their upregulation in several pathologies[10,11] has motivated the design of reporters and therapeutics that can be targeted by local protease activation, with demonstrated success *in vivo*.[12−16] Interestingly, viruses are known to depend on proteolytic processing for various steps of their life cycle, including capsid maturation, membrane fusion, and uncoating,[17−20] indicating proteases are a class of biomolecular inputs natural to virus systems. Prior efforts have engineered retrovirus[14] and measles virus,[13] both enveloped viruses, to become activated by single target proteases. We sought to expand upon prior groundwork by engineering proteolytic regulation into the protein capsid of AAV such that its gene delivery function can be controlled by the signal integration of multiple protease inputs. Specifically, we desired the capsid to require two different protease inputs in order to activate the virus, similar to how a digital AND gate operates. As a proof-of-concept, we set out to design AAV serotype 2 (AAV2) to be activated by matrix metalloproteinases (MMPs)-2, -7, and -9, since gene delivery vectors responsive to these enzymes may have applications in biomedicine.[10−16]

RESULTS AND DISCUSSION

To build viruses able to "compute" protease inputs as a requisite of gene delivery (Figure 1a), we developed a design strategy involving the genetic insertion of small

* Address correspondence to jsuh@rice.edu.

Received for review January 27, 2014 and accepted April 30, 2014.

Published online May 05, 2014
10.1021/nn500550q

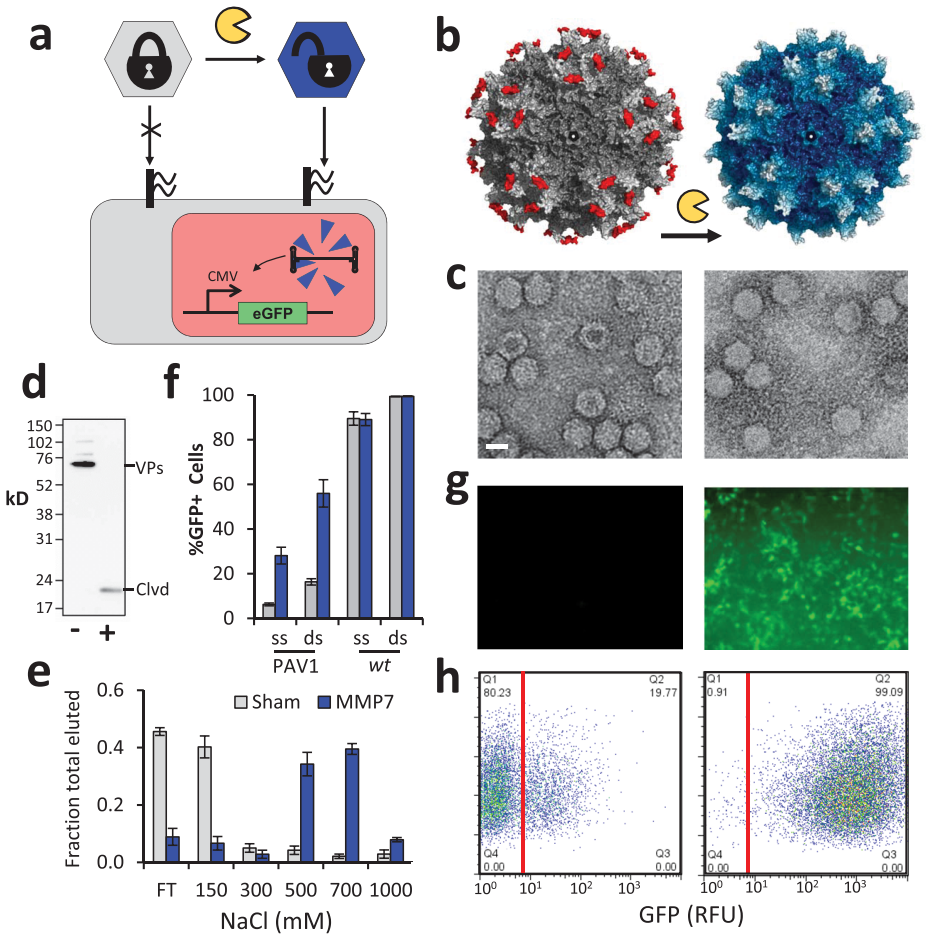

Figure 1. Programming AAV capsid with proteolytic regulation. (a) Operation of PAVs. Locked virus cannot interact with cellular HSPG until processed by target protease. Upon virus activation, genetic payload (CMV-GFP transgene) is delivered to cell nucleus. (b) Molecular models of PAV1 (Table 1) in locked (gray) and unlocked (blue) states. Peptide lock leaving group in red. (c) Electron micrographs of PAV1 in the locked (left) and unlocked (right) states indicate capsids remain intact after MMP-7 treatment (scalebar = 20 nm). (d) Western blot with B1 antibody shows cleaved VP after MMP-7 (+) treatment compared to sham (−). (e) Heparin chromatography reveals low-affinity uncleaved virus (gray) elutes in low salt, whereas MMP-7 treated particles require high ionic strength to disrupt tight AAV-heparin interactions. (f) HEK293T cells transduced (gMOI = 700) by PAV1 capsids, packaging a single-stranded (ssDNA) or a self-complementary double-stranded (dsDNA) transgene,[30] show striking increases in gene delivery after treatment by MMP-7 (blue bars) compared to sham (gray bars). Expectedly, the dsDNA transgene increases gene expression from both sham and MMP-7 treated PAV1. *Wt* capsids shown for comparison (note: dsDNA is saturated at approximately 100% GFP+ cells). (g, h) MMP-7 treated PAV at right, sham at left. (g) Fluorescent micrographs of HEK293T cells transduced with PAV1 (ssDNA) before/after MMP-7 treatment. (h) Dotplots of HEK293T cells transduced by PAV12 (dsDNA, gMOI = 1000). Error bars are SEM from two (panel e) and three (panel f) independent experiments, each performed in duplicate.

peptide "locks" into the capsid. Since the interactions between AAV2 and heparan sulfate proteoglycans (HSPGs) are driven by electrostatic forces,[21,22] we rationalized that small highly charged peptides could interfere with this virus−receptor interaction. Thus, we designed a small peptide lock (Lock1; Figure 1b, Table 1) containing a negatively charged tetra-aspartic acid motif (D_4) flanked by a pair of proteolytically cleavable peptides (PLGLAR, sensitive to MMPs)[23] and spaced by glycine/alanine linkers. Lock insertion was expected to inactivate the virus by preventing binding to cell surface receptors, and removal of the peptide *via* proteolysis should allow the virus to regain its cell binding and gene delivery functionality. To generate an effective lock, insertion into the capsid must satisfy the following design criteria: (1) preservation of capsid assembly and genome packaging, (2) interference of virus-receptor interactions, (3) surface accessibility for efficient proteolytic processing, and (4) recovery of heparin/HSPG affinity after proteolysis.

We posited that genetic insertion of the peptide lock near the quaternary HSPG binding domain (HBD) could enable effective regulation of virus−receptor interactions. To identify potential sites for insertion, an alignment of homologous AAV serotypes (Figure S1, Supporting Information) was used to identify two nonconserved residues near the HBD, G453, and G586, which are surface accessible and tolerant to mutation.[24,25] Genetic insertion of Lock1 after G453 yields intact, packaged capsids with a surface-displayed MMP-7 cleavable

TABLE 1. PAV locks.[a]

Virus ID	Lock ID	Lock Sequence	MMP2*	MMP7*	MMP9*
PAV1	L1	AG-PLG↓LAR-G-DDDD-G-PLG↓LAR-GA	-	++	+
PAV18	L18	AG-VPMS↓MRGG-G-DDDD-G-VPMS↓MRGG-GA	+	+	++
PAV12	L12	AG-IPES↓LRAG-G-DDDD-G-IPES↓LRAG-GA	-	++	-
PAV10	L10	AGGG-GPQG↓IAGQ-G-DDDD-G-GPQG↓IAGQ-GRGA	-	-	+

*$A_{1/2}$ reached after 4 h, 37 °C at [MMP]: ++ ≥ 100 nM; + ≥ 316 nM; - Not activated

[a] Lock sequences used for PAVs. Known cleavage sequences[23,26] underlined and leaving groups in red. At right, relative sensitivity of PAVs to MMPs corresponding to data in Figure 2. *$A_{1/2}$ reached after 4 h, 37 °C at [MMP]: ++, >100 nM; +, >316 nM; −, not activated.

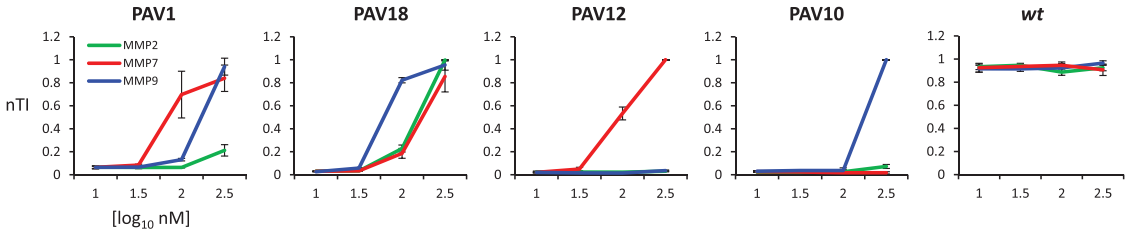

Figure 2. PAV variants display different susceptibilities to MMPs. PAVs treated with MMP-2, -7, or -9 were used to transduce HEK293T cells with a GFP reporter (dsDNA). *Y*-axes indicate normalized transduction index (nTI) as a measure of virus activity. Sample sizes of independent experiments performed in duplicate: PAV1, *n* = 4; PAV18, *n* = 2; PAV12, *n* = 3; PAV10, *n* = 2; wt, *n* = 3. Error bars are SEM.

peptide, but AAV−heparin interactions are not disrupted (Figure S2, Supporting Information). In contrast, insertion after G586—between two critical HSPG binding residues R585 and R588[21]—effectively ablates heparin affinity (Figure 1e). Strikingly, treatment of PAV1 (protease-activatable virus 1) with MMP-7 results in effective lock cleavage and recovery of heparin affinity (Figure 1d, e). Application of PAV1 (activated vs unactivated) to HEK293T cells demonstrates that regulation of PAV−HSPG interactions translates to effective protease-modulated gene delivery *in vitro* (Figure 1f−h) with up to 100-fold increase in cellular transduction (Figure S3, Supporting Information). This effect is specific to PAVs, since *wt* capsids are not affected by treatment with any MMP tested (Figure 2). A molecular model of PAV1 illustrates a possible conformation the anionic peptide lock may assume, hovering over the cationic HBD (Figure 1b). These results show AAV−receptor interactions can be modulated by a target protease.

To test the modularity of the PAV lock device, we sought to create mutants exhibiting altered specificities. A panel of PAV variants was constructed by replacing the cleavage motif of Lock1 with previously identified sequences having demonstrated susceptibility to different MMPs (Table 1).[26] The susceptibilities of PAVs to various concentrations of MMPs-2, -7, and -9 were then tested (Figure 2). Our results indicate PAV1 and PAV18 are promiscuous to these MMPs, though their response to each protease varies. On the other hand, PAV10 (MMP-9 responsive) and PAV12 (MMP-7 responsive) exhibit a high degree of selectivity among the proteases tested. These results demonstrate AAV capsids can be designed to accept a range of protease inputs and their response to closely related proteases can be tuned to achieve a high degree of specificity to single protease inputs.

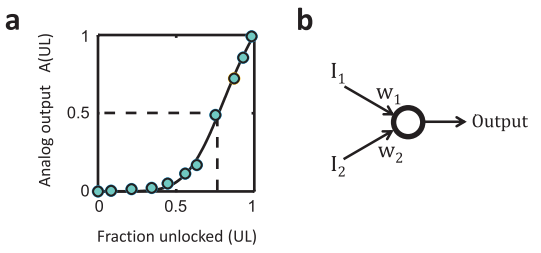

Figure 3. PAV activation dynamics and transfer function. (a) Transfer function of analogue PAV activity A(UL) (mean relative transduction index, cyan circles) as a function of fraction unlocked (UL), fit to Hill function (eq 2; *n* = 5.8, *K* = 0.85). Threshold (dashed line) required to achieve 50% activation ($A_{1/2}$) is shown (*t* = 0.77; *i.e.* ∼46 unlocked peptides or >90 single cleavage events per capsid). (b) Nodal abstraction of PAVs integrating multiple inputs (l_i = fraction unlocked of lock type L_i) with tunable weights (w_i), generating output virus activity through transfer function in (a).

To gain mechanistic insight into how PAVs respond to proteolytic processing, we determined the transfer function of the relative activity of PAV1 in response to varying degrees of cleavage by MMP-9 (Figure 3a and Figures S4−S6, Supporting Information). Here, we compared the fraction of peptides unlocked (cleaved at both protease sensitive motifs) to the virus' activity on HEK293T cells. As would be expected from

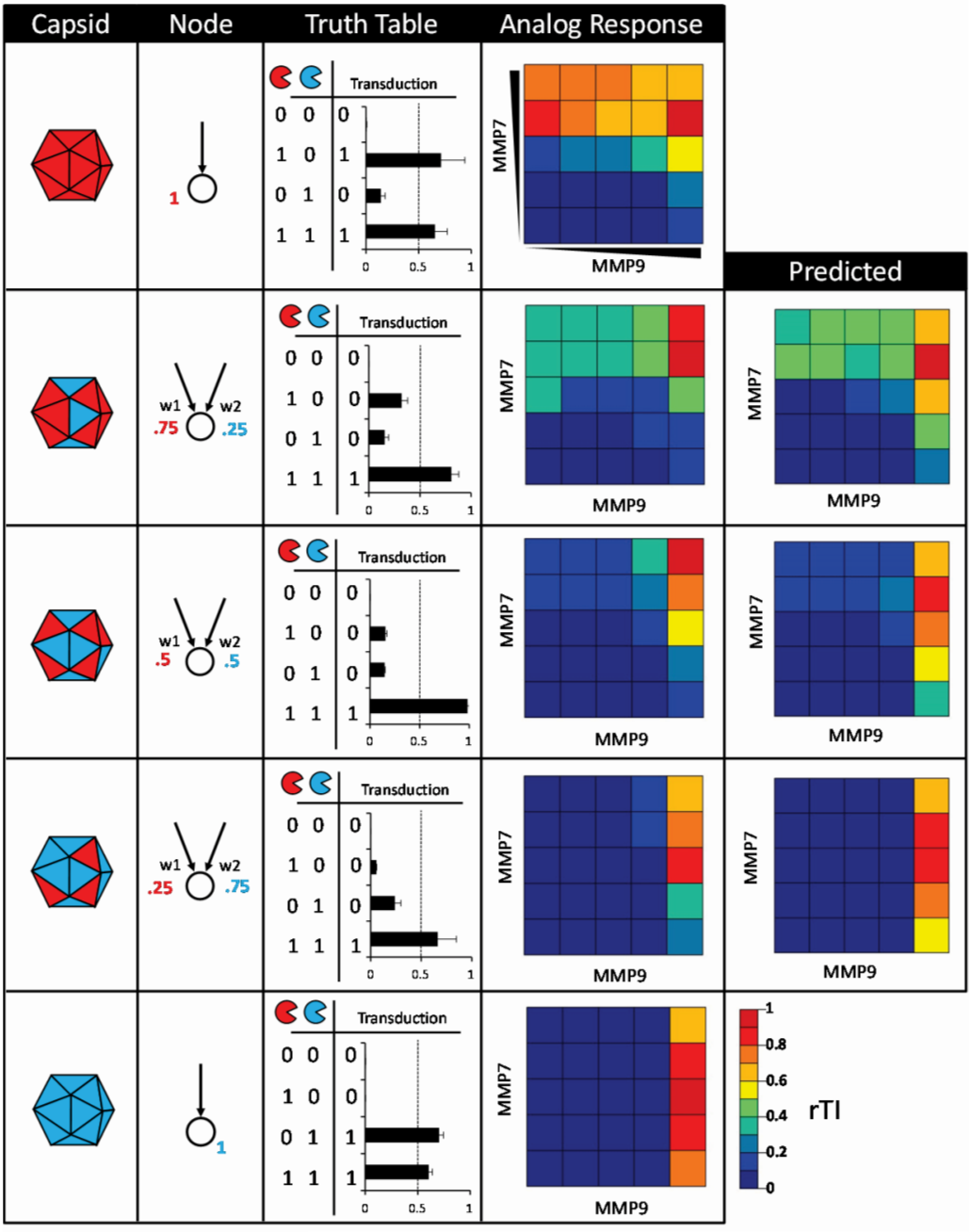

Figure 4. Tunable PAVs built from mosaic capsids. PAV12 (top, all red capsid) and PAV10 (bottom, all blue capsid) are single-input devices (MMP-7 and MMP-9, respectively). Mosaic capsids (middle three rows) composed of subunits from PAV12/10 (weights indicated by nodal diagrams) demonstrate tunability of devices. Analogue response column shows experimentally obtained heat maps of virus activity (in relative TI, rTI) to different combinations of MMP inputs (0, 1, 1.5, 2, 2.5 $\log_{10}$ nM, 4 h at 37 °C). Bar graphs show the analogue response (in rTI) can be simplified to adhere to a binary AND gate truth table (Inputs: 0 = sham, 1 = $10^{2.5}$ nM MMP) by using $A_{1/2}$ as an activation threshold (dashed line), where 0.5/0.5 mosaic performs optimally. Predicted mosaic responses are calculated from pure capsid (entirely PAV12 or PAV10) responses using eqs 1 and 2. Unzeroed data available in Figure S10, Supporting Information. Sample sizes of independent experiments performed in duplicate (top to bottom): n = 2,3,3,2. Truth table error bars show SEM.

polyvalent receptor–ligand avidity,[27] the transfer function shows a nonlinear increase in gene delivery with respect to the fraction of unlocked peptides. However, the shape of the transfer function reveals that transduction activity does not reach maximum until nearly all peptide locks are removed from the capsid. It is unclear that this type of behavior is due to virus-receptor avidity effects alone. Other factors that may be contributing to the PAV transfer function include altered coreceptor interactions, intracellular trafficking or uncoating. Quantification of virus internalization at different states of PAV activation reveals the increased gene delivery in response to proteolysis is due mainly to increased cell entry (Figure S8, Supporting Information).

Further work will be required to elucidate fully the key steps that contribute to PAV transduction efficiency in response to proteolytic processing.

The nonlinear dynamics of PAV activation—with respect to fraction peptides unlocked—revealed that we may be able to program multiple input signal integration by creating mosaic[28] PAV capsids containing subunits from PAV variants that are activated by different MMPs. We hypothesized such mosaic capsids could display AND gate Boolean logic when built using a mixture of PAV12 and PAV10 capsid subunits, since a mosaic capsid containing these subunits would require both locks (L12 and L10) receive their specific inputs (MMP-7 and MMP-9, respectively) to achieve mosaic virus activation. To better conceptualize this idea, we considered how a mosaic PAV capsid acts as a node by integrating different proteolytic inputs to generate transduction activity as an output (Figure 3b):

$$\text{input}: \text{UL} = \Sigma l_i w_i \quad (1)$$

$$\text{output}: A(\text{UL}) = \frac{(K^n + 1)\text{UL}^n}{K^n + \text{UL}^n} \quad (2)$$

Here, the input function UL eq 1 describes the fraction of total peptides unlocked in a PAV capsid which equals a weighted sum of the fraction unlocked (l_i) of each subunit type. The weights (w_i) indicate the fraction of the capsid composed of each subunit type, which sum to 1. For example, a mosaic capsid composed of a 1:1 ratio of PAV12 and PAV10 subunits is represented by weights $w_i = 0.5$ for each subunit type. The output transfer function A(UL) describes the relative PAV activity (relative transduction index) as a function of UL. Although the Hill function is typically used to model cooperative molecular binding, we used it here to describe the apparent cooperativity of PAV activity with respect to UL, allowing us to predict mosaic PAV responses given proteolytic inputs l_i.

According to this model, an AND gate can be built by combining two highly specific subunits weighted equally at 0.5/0.5 (Figure S9, Supporting Information), since the output A(UL) is negligible when only one subunit lock type (L_i) is fully cleaved. However, when both lock types are cleaved in the presence of their preferred proteases, cellular transduction is predicted to be synergistically higher. To test this hypothesis, we generated mosaic capsids from PAV12 and PAV10 expressed at a 1:1 ratio (PAV12/10). Assuming capsid assembly follows a binomial process (n = 60 subunits), >99% capsids should contain at least 21 copies of each subunit type. Thus, even when one subunit type is fully cleaved, there remain at least 21 uncleaved subunits in nearly all PAVs, keeping them in the locked state. Figure 4 shows the mosaic PAV12/10 operating as an AND gate, as it requires high levels of both MMP-7 and MMP-9 to achieve activation beyond 50% relative PAV activity ($A_{1/2}$). If the ratios of the capsid subunits are adjusted, the PAV response can be tweaked toward the dominant subunit. Remarkably, the data from single-input virus nanoparticles (*i.e.*, PAV12 and PAV10) can be used to predict the experimental output response surfaces of the various mosaic PAVs (Figure 4 and Supplemental Methods).

CONCLUSIONS

The virus nanonodes described in this work represent a new class of molecularly engineered gene vectors. Their operation is unique in that each nanoparticle has the potential to integrate multiple proteolytic inputs. We have shown Boolean AND gate logic can easily be programmed using mosaic capsids and the analogue response to different protease signatures can be tuned by altering the weights of each lock type. Further investigation will be required to uncover the full capacity of PAV signal integration. For example, the requirement that both upstream and downstream cleavage sites must be engaged for PAV activation may enable expansion of signal integration with nested AND gate architectures. Our ability to predictably design mosaic PAVs to obtain desired responses will assist future developments of this technology. The output of PAV devices—gene delivery—is a clinically useful tool that can now potentially be controlled by combinatorial signatures of proteases which serve as biomarkers in a number of pathologies.

METHODS

Virus Production. All PAV plasmids were generated from a modified pRC_RR[29] containing linkers for ligation to locks using NgoM IV and Kas I sites at positions 586 and 453. Various locks were generated by annealing and phosphorylating synthesized oligonucleotides (Integrated DNA Technologies, Coralville, IA). These derivatives were used as packaging plasmids, along with a GFP transgene (single-stranded: pAAV_GFP, double-stranded: scAAV2-CMV-GFP) and helper plasmids (XX6-80) to produce viruses as previously described.[29] Mosaic capsids were generated by altering the molar ratio of packaging plasmids. Density gradient purification was followed by anion exchange chromatography (Q Sepharose, Pall) and buffer exchange by Amicon Ultra 4 (Millipore) into GB-PF68 (50 mM Tris, pH 7.6, 150 mM NaCl, 10 mM MgCl2, 0.001% Pluronic F68). Purified viruses are stable at 4 °C in this buffer for several months in low retention microtubes from Phenix Research (Candler, NC).

Proteolysis of PAVs. MMP-2, MMP-7, and MMP-9 were purchased from Enzo Life Sciences (Farmingdale, NY). Viruses were diluted in reaction buffer (50 mM Tris-Cl, pH 7.4, 150 mM NaCl, 10 mM $MgCl_2$, 10 mM $CaCl_2$) prior to addition of 9X protease, diluted to 9X in their storage buffer (50 mM Tris, pH 7.5, 300 mM NaCl, 5 mM $CaCl_2$, 10 μM $ZnCl_2$, 0.5% Brij-35, 30% glycerol). Unless noted, reactions were carried out with 100 nM protease at 37 °C for 4 h and stopped with 25 mM EDTA. Virus particles were stable under these conditions for days at 37 °C and weeks at 4 °C.

Protease activity was calibrated prior to each experiment to reduce variability due to enzyme storage and to facilitate future replication of work. Briefly, enzyme activity was measured using

the fluorogenic substrate Mca-PLGL-Dpa-AR (Calbiochem) and a Tecan M1000 plate reader at 5 nM enzyme and 5 μM substrate in 50 mM Tris, pH 7.4, 150 mM NaCl, 5 mM $CaCl_2$, 0.05% Brij-35. Initial reaction velocities were used to standardize each proteolysis assay to a representative preliminary kinetic measurement (MMP-2 = 0.94, MMP-7 = 0.88, MMP-9 = 0.15 nM/s). Reported concentrations in this manuscript assumed these preliminary measurements represent the enzyme concentrations listed by the manufacturer.

Transduction assay. Viruses were produced as described previously[29] and in the Supplemental Methods (Supporting Information). HEK293T cells were seeded at 1×10^5 cells/well on poly-L-lysine-coated 48-well plates 36 h before transduction, which was performed in serum-free media. Media was refreshed (with serum) at 12 h post-transduction and harvested at 48 h for flow cytometry on a BD FACSCanto II.

Transduction index (TI = % GFP+ cells x geometric mean fluorescence intensity) is a linear indicator of relative virus activity (Figure S7, Supporting Information). In Figure 2, normalized transduction index (nTI) was computed by dividing TI by maximum TI in each experiment to adjust for differences due to cell culture variability; thus, error for maximal values for PAV 12 and PAV10 cannot be computed. In Figures 3 and 4, TI was zeroed by subtracting sham before normalizing to max level, yielding relative TI (rTI).

Electron Microscopy. Virus samples were applied to glow-discharged, 300 mesh continuous carbon sample grids (Ted Pella) for 5 min. Grids were dried by contact with filter paper wicks and washed twice in ultrapure water. Negative staining was then performed for 20 s in uranyl formate (7.5 mg/mL). Images were taken with a JEM FasTEM 2010 transmission electron microscope at 120000× magnification.

Conflict of Interest: The authors declare no competing financial interest.

Supporting Information Available: Supplemental methods and supplemental data. This material is available free of charge *via* the Internet at http://pubs.acs.org.

Acknowledgment. We thank M. Weitzman and J. Tabor for critical review of the manuscript and M. Diehl for scientific discussions. We also acknowledge the University of North Carolina at Chapel Hill Gene Therapy Center Vector Core for providing us with pXX2, pXX6-80, and scAAV2-CMV-GFP. This material is based upon work supported by the National Science Foundation under Grant No. 0955536, National Institutes of Health under Grant Nos. P50-CA083639 and U54CA151668, American Heart Association under Grant No. 13GRNT14420044, and Cancer Prevention and Research Institute of Texas under Grant No. RP130455 to J.S., and National Institutes of Health under Grant No. R01GM082946 to M.A.M.

REFERENCES AND NOTES

1. Park, S. H.; Zarrinpar, A.; Lim, W. A. Rewiring MAP Kinase Pathways Using Alternative Scaffold Assembly Mechanisms. *Science* **2003**, *299*, 1061–1064.
2. Lee, Y. J.; Yi, H.; Kim, W. J.; Kang, K.; Yun, D. S.; Strano, M. S.; Ceder, G.; Belcher, A. M. Fabricating Genetically Engineered High-Power Lithium-Ion Batteries Using Multiple Virus Genes. *Science* **2009**, *324*, 1051–1055.
3. Miller, R. A.; Presley, A. D.; Francis, M. B. Self-Assembling Light-Harvesting Systems from Synthetically Modified Tobacco Mosaic Virus Coat Proteins. *J. Am. Chem. Soc.* **2007**, *129*, 3104–3109.
4. Lee, B. Y.; Zhang, J.; Zueger, C.; Chung, W. J.; Yoo, S. Y.; Wang, E.; Meyer, J.; Ramesh, R.; Lee, S. W. Virus-Based Piezoelectric Energy Generation. *Nat. Nanotechnol* **2012**, *7*, 351–356.
5. Lewis, J. D.; Destito, G.; Zijlstra, A.; Gonzalez, M. J.; Quigley, J. P.; Manchester, M.; Stuhlmann, H. Viral Nanoparticles as Tools for Intravital Vascular Imaging. *Nat. Med.* **2006**, *12*, 354–360.
6. Comellas-Aragones, M.; Engelkamp, H.; Claessen, V. I.; Sommerdijk, N. A. J. M.; Rowan, A. E.; Christianen, P. C. M.; Maan, J. C.; Verduin, B. J. M.; Cornelissen, J. J. L. M.; Nolte, R. J. M. A Virus-Based Single-Enzyme Nanoreactor. *Nat. Nanotechnol* **2007**, *2*, 635–639.
7. Lucon, J.; Qazi, S.; Uchida, M.; Bedwell, G. J.; LaFrance, B.; Prevelige, P. E., Jr.; Douglas, T. Use of the Interior Cavity of the P22 Capsid for Site-Specific Initiation of Atom-Transfer Radical Polymerization with High-Density Cargo Loading. *Nat. Chem.* **2012**, *4*, 781–788.
8. Ortiz, M. E.; Endy, D. Engineered Cell-Cell Communication *via* DNA Messaging. *J. Biol. Eng.* **2012**, *6*, 16.
9. Turk, B.; Turk, D.; Turk, V. Protease Signalling: the Cutting Edge. *EMBO J.* **2012**, *31*, 1630–1643.
10. Egeblad, M.; Werb, Z. New Functions for the Matrix Metalloproteinases in Cancer Progression. *Nat. Rev. Cancer* **2002**, *2*, 161–174.
11. Sbardella, D.; Fasciglione, G. F.; Gioia, M.; Ciaccio, C.; Tundo, G. R.; Marini, S.; Coletta, M. Human Matrix Metalloproteinases: An Ubiquitarian Class of Enzymes Involved in Several Pathological Processes. *Mol. Aspects Med.* **2012**, *33*, 119–208.
12. Savariar, E. N.; Felsen, C. N.; Nashi, N.; Jiang, T.; Ellies, L. G.; Steinbach, P.; Tsien, R. Y.; Nguyen, Q. T. Real-time *in Vivo* Molecular Detection of Primary Tumors and Metastases with Ratiometric Activatable Cell-Penetrating Peptides. *Cancer Res.* **2013**, *73*, 855–864.
13. Springfeld, C.; von Messling, V.; Frenzke, M.; Ungerechts, G.; Buchholz, C. J.; Cattaneo, R. Oncolytic Efficacy and Enhanced Safety of Measles Virus Activated by Tumor-Secreted Matrix Metalloproteinases. *Cancer Res.* **2006**, *66*, 7694–7700.
14. Peng, K.; Morling, F.; Cosset, F.; Murphy, G.; Russell, S. A Gene Delivery System Activatable by Disease-Associated Matrix Metalloproteinases. *Hum. Gene Ther.* **1997**, *8*, 729–738.
15. Jiang, T.; Olson, E. S.; Nguyen, Q. T.; Roy, M.; Jennings, P. A.; Tsien, R. Y. Tumor Imaging by Means of Proteolytic Activation of Cell-Penetrating Peptides. *Proc. Natl. Acad. Sci. U.S.A.* **2004**, *101*, 17867–17872.
16. Erster, O.; Thomas, J. M.; Hamzah, J.; Jabaiah, A. M.; Getz, J. A.; Schoep, T. D.; Hall, S. S.; Ruoslahti, E.; Daugherty, P. S. Site-Specific Targeting of Antibody Activity *in Vivo* Mediated by Disease-Associated Proteases. *J. Controlled Release* **2012**, *161*, 804–812.
17. McCune, J. M.; Rabin, L. B.; Feinberg, M. B.; Lieberman, M.; Kosek, J. C.; Reyes, G. R.; Weissman, I. L. Endoproteolytic Cleavage of gp160 is Required for the Activation of Human Immunodeficiency Virus. *Cell* **1988**, *53*, 55–67.
18. Greber, U. F.; Webster, P.; Weber, J.; Helenius, A. The Role of the Adenovirus Protease on Virus Entry into Cells. *EMBO J.* **1996**, *15*, 1766–1777.
19. Lazarowitz, S. G.; Choppin, P. W. Enhancement of the Infectivity of Influenza A and B Viruses by Proteolytic Cleavage of the Hemagglutinin Polypeptide. *Virology* **1975**, *68*, 440–454.
20. Chandran, K.; Sullivan, N. J.; Felbor, U.; Whelan, S. P.; Cunningham, J. M. Endosomal Proteolysis of the Ebola Virus Glycoprotein Is Necessary for Infection. *Science* **2005**, *308*, 1643–1645.
21. O'Donnell, J.; Taylor, K. A.; Chapman, M. S. Adeno-Associated Virus-2 and Its Primary Cellular Receptor--Cryo-EM Structure of a Heparin Complex. *Virology* **2009**, *385*, 434–443.
22. Levy, H. C.; Bowman, V. D.; Govindasamy, L.; McKenna, R.; Nash, K.; Warrington, K.; Chen, W.; Muzyczka, N.; Yan, X.; Baker, T. S.; et al. Heparin Binding Induces Conformational Changes in Adeno-Associated Virus Serotype 2. *J. Struct Biol.* **2009**, *165*, 146–156.
23. Knight, C. G.; Willenbrock, F.; Murphy, G. A Novel Coumarin-Labelled Peptide for Sensitive Continuous Assays of the Matrix Metalloproteinases. *FEBS Lett.* **1992**, *296*, 263–266.
24. Wu, P.; Xiao, W.; Conlon, T.; Hughes, J.; Agbandje-McKenna, M.; Ferkol, T.; Flotte, T.; Muzyczka, N. Mutational Analysis of the Adeno-Associated Virus Type 2 (AAV2) Capsid Gene and Construction of AAV2 Vectors with Altered Tropism. *J. Virol.* **2000**, *74*, 8635–8647.
25. Girod, A.; Ried, M.; Wobus, C.; Lahm, H.; Leike, K.; Kleinschmidt, J.; Deleage, G.; Hallek, M. Genetic Capsid Modifications Allow

Efficient Re-Targeting of Adeno-Associated Virus Type 2. *Nat. Med.* **1999**, *5*, 1052–1056.
26. Turk, B. E.; Huang, L. L.; Piro, E. T.; Cantley, L. C. Determination of Protease Cleavage Site Motifs Using Mixture-Based Oriented Peptide Libraries. *Nat. Biotechnol.* **2001**, *19*, 661–667.
27. Krishnamurthy, V. M.; Estroff, L. A.; Whitesides, G. M., Multivalency in Ligand Design. In *Fragment-Based Approaches in Drug Discovery*; Wiley-VCH: Weinheim, 2006; pp 11−53.
28. Gigout, L.; Rebollo, P.; Clement, N.; Warrington, K. H.; Muzyczka, N.; Linden, R. M.; Weber, T. Altering AAV Tropism with Mosaic Viral Capsids. *Mol. Ther* **2005**, *11*, 856–865.
29. Judd, J.; Wei, F.; Nguyen, P. Q.; Tartaglia, L. J.; Agbandje-McKenna, M.; Silberg, J. J.; Suh, J. Random Insertion of mCherry Into VP3 Domain of Adeno-associated Virus Yields Fluorescent Capsids With no Loss of Infectivity. *Mol. Ther.—Nucleic Acids* **2012**, *1*, e54.
30. Wang, Z.; Ma, H. I.; Li, J.; Sun, L.; Zhang, J.; Xiao, X. Rapid and Highly Efficient Transduction by Double-Stranded Adeno-Associated Virus Vectors *In Vitro* and *In Vivo*. *Gene Ther.* **2003**, *10*, 2105–2111.